Clay Minerals (2005) **40**, 511–522

Structural modifications of smectites mechanically deformed under controlled conditions

G. E. CHRISTIDIS[1,*], F. DELLISANTI[2], G. VALDRE[2] AND P. MAKRI[1]

[1] *Technical University of Crete, Department of Mineral Resources Engineering, 73100 Chania, Greece, and*
[2] *Dipartimento di Scienze della Terra e Geo-Ambientali, Universita di Bologna, Piazza di Porta S. Donato, I 40126 Bologna, Italy*

(*Received 8 June 2005; revised 14 September 2005*)

ABSTRACT: SWy-1 and SAz-1 smectites and an Italian bentonite from Sardinia were mechanically deformed via high-energy ball milling for 20 h, in a controlled thermodynamic environment at constant temperature (25ºC) under vacuum. The deformed smectites have a lower cation exchange capacity (CEC) and form thicker particles than the original ones, due to agglomeration of smectite crystallites. The 001 diffraction maximum shifted to lower *d* spacings, the intensity of the 060 reflection decreased and the background at 20–30º2θ increased, suggesting partial amorphization of the smectite. Moreover, the layer charge of the smectites decreased. The intensity of the complex stretching band at 3625 cm^{-1}, and the AlAlOH, and $AlFe^{3+}OH$ bending bands at 916 cm^{-1} and 886 cm^{-1}, respectively, decreased, while the band at AlMgOH bending at 849 cm^{-1}, disappeared. Deformation mainly disrupted the octahedral sheet and preferentially destroyed those sites occupied by Mg cations, thus explaining the observed decrease in layer charge. Octahedral sites occupied by Fe were least affected. The disruption of the octahedral sheet is substantiated further by the almost total disappearance of the dehydroxylation peak, which is more pronounced in the Mg-rich SAz-1 smectite.

KEYWORDS: mechanical deformation, grinding, amorphization, smectite, layer charge, CEC.

Grinding is known to affect the structure and properties of various clay minerals used as industrial fillers such as kaolinite (Gregg, 1968; Kristoff *et al.*, 1993; Suraj *et al.*, 1997; Stepkowska *et al.*, 2001), talc (Mukherjee & Roy, 1973; Liao & Senna, 1992; Sanchez-Soto *et al.*, 1997; Christidis *et al.*, 2004), pyrophyllite (Perez-Rodriguez & Sanchez-Soto, 1991; Wiewióra *et al.*, 1993; Uhlik *et al.*, 2000), and smectite (Mingelgrin *et al.*, 1978; Čičel & Kranz, 1981; Volzone *et al.*, 1987; Christidis *et al.*, 2004). In most cases grinding causes delamination in initial stages followed by destruction of the structure and subsequent amorphization, associated with re-aggregation (cold welding according to Gregg, 1968) of the mineral grains (Sanchez-Soto *et al.*, 1997; Stepkowska *et al.*, 2001, among many others). Reynolds & Bish (2002) showed that progressive grinding of kaolinite produces increased amounts of disordered kaolinite, coexisting with relatively unaffected material. Nevertheless, there are exceptions to this trend: Christidis *et al.* (2004) showed that controlled grinding of smectite for up to 90 min may proceed with progressive decrease of grain size without considerable structural modifications at the crystallite size level.

Most clay minerals used as industrial fillers or coatings are ground excessively, to a final grain

* E-mail: christid@mred.tuc.gr
DOI: 10.1180/0009855054040188

size usually <5 μm, because particle size affects important properties such as colour (Scott, 1990; Christidis *et al.*, 2004) and rheology (Brandenburg & Lagaly, 1988; see Güven, 1988, for a review). The greater problem during grinding is that most of the energy consumed is absorbed by the grinding device itself and only a tiny fraction (~1%) is available for size comminution (Wills, 1988). Thus most energy is utilized in the production of heat during grinding. Since grinding produces new mineral surfaces, the modifications observed in the structure of clay minerals after grinding are expected to result from mechanical breaking of the grains and from production of heat. Both these factors control particle agglomeration usually observed after prolonged grinding (e.g. Sanchez-Soto *et al.*, 1997; Stepkowska *et al.*, 2001). Thus the broken bonds created during comminution enhance attraction between the grains. The latter is favoured by the development of heat in the grinding circuits.

Recently, Dellisanti & Valdre (2005) ground a Sardinian smectite in a ball mill under medium vacuum of 0.13 Pa and controlled temperature conditions (25ºC) achieved by specially built, air-cooled mechanical jar reactors. Although the smectite structure displayed degradation it was retained even after 20 h of continuous grinding, without considerable amorphization. Therefore, controlled grinding could be used to produce end products with tailored properties. In this study we examine the influence of grinding, in a controlled environment, on the layer charge of three bentonites containing smectites with different layer charge and charge distribution, and we attempt to evaluate the influence of layer charge and charge distribution on the structural modification of smectites. The data will be useful for the prediction of physical properties of smectites in various industrial applications.

MATERIALS AND METHODS

The bentonites examined are SWy-1 and SAz-1 obtained from The Clay Minerals Society's Source Clays repository and a bentonite from Sardinia, Italy. The mineralogy of the original and the deformed (ground) samples was studied by X-ray diffraction (XRD) using a Philips PW 1710 diffractometer, with Cu-$K\alpha$ radiation, a graphite monochromator, 40 kV/30 mA, 1º divergence and detector slits, 0.02 scanning step and 10 s counting time per step. The Sardinian bentonite consists of smectite (>90%) and minor feldspar and clinoptilolite (Dellisanti & Valdre 2005). According to Pietracaprina *et al.* (1971) the smectite in the bentonite of Uri, NW Sardinia, is a montmorillonite with ~16% tetrahedral charge. SWy-1 contains low-charge montmorillonite with 30% tetrahedral charge, minor quartz, K-feldspar, calcite and illite. SAz-1 contains a high-charge montmorillonite (>95%) with almost entirely octahedral charge (Otay-type montmorillonite according to Schultz (1969) and Newman & Brown (1987)) and trace quartz (~1%).

The clay mineralogy of the bentonites was determined using oriented clay fractions. The smectites were dispersed in distilled water using an ultrasonic probe (20 s). The <2 μm fractions were separated by settling, dried on glass slides, allowed to dry at room temperature and solvated with ethylene-glycol vapour at 60ºC overnight. Both the air-dried and the ethylene-glycol solvated samples were examined by XRD. The layer charge and charge distribution of the smectites before and after mechanical treatment was determined by the LayerCharge program (Christidis & Eberl, 2003) on the K-saturated, ethylene glycol solvated clay fractions of the bentonites. The method calculates the magnitude of the layer charge and the extent of layer-charge distribution from the relative proportions of low-charge (17 Å), intermediate-charge (13.5 Å), and high-charge (9.98 Å) layers, by assuming that K-smectites consist of fully swelling, partially swelling and non-swelling layers.

Grinding of the bentonites was carried out using a planetary ball mill (Pulverisette 5, Fritsch, Germany). Milling was performed in medium vacuum of 0.13 Pa (10^{-3} Torr) at 25ºC using specifically built air-cooled mechanical jar-reactors (maximum operational temperature of <50ºC), as already successfully used for mechanical deformation of other compounds and minerals (Bonetti *et al.*, 1998; Valdrè *et al.*, 1999).

The structural modifications of the smectites after mechanical deformation were determined with infrared spectroscopy using a Nicolet Avatar 360 Fourier Transform Infrared (FTIR) spectrometer in the range 400−4000 cm^{-1}. 1 mg of each sample was diluted in 200 mg of KBr and pressed into 13 mm pellets. Before analysis the pellets were heated at 100ºC overnight. Differential thermal analysis-thermogravimetric analysis (DTA-TGA) analysis of the original and the deformed samples was carried out with a Setaram TAG24 DTA-TG

thermal analyser in the temperature range 50–1200ºC, with a heating rate of 10ºC/min using a helium atmosphere. The CEC of the original and the deformed bentonites was measured in duplicate with ammonium saturation (1 N ammonium acetate at pH 7), Kjeldahl distillation and titration of the evolved ammonia with 0.05 N H_2SO_4 using methyl red and bromocresol green indicators. The standard deviation of the CEC measurements is 0.3 mEq/100 g.

Particle-size measurements of the original and ground bentonite samples were carried out by laser diffraction using a Malvern© particle-size analyser. Laser diffraction measures the mean size of deflocculated bentonite suspensions and provides the particle-size distribution of the suspended particles. The mean grain size (d_v) measured by laser diffraction corresponds to a sphere having the same volume as the grain (Allen, 1990). Finally, adsorption-desorption isotherms of the original and the deformed bentonites were obtained by N_2 gas adsorption using a NOVA 2200 surface area analyser (Quantachrome). Samples were outgassed overnight at 140ºC under a vacuum of 1.3 Pa (10^{-2} Torr). Specific surface area (SSA) was determined by BET equation (Brunauer *et al.*, 1938) using the P/P_0 range 0–0.35 of the adsorption branch of the isotherms, while pore-size distribution was determined from the desorption branch of the isotherms.

RESULTS

Influence of grinding on smectite structure

Deformation after 20 h of ball milling of the bentonites caused disruption of the basal surfaces (more intense in the SAz-1 smectite), decrease in the layer charge of smectites, agglomeration of smectite grains and partial amorphization. Note that previous work has shown that grinding of bentonites for considerably shorter time (i.e. up to 3 h) using conventional oscillating mills caused almost total disappearance of the basal reflections and extensive amorphization (Čičel & Kranz, 1981; Volzone *et al.*, 1987). The influence on the smectite structure can be seen in Fig. 1. The intensity of the basal spacings of all smectites decreases significantly and the peak migrates to higher 2θ angles. This effect is more pronounced in the case of SWy-1. Also, in all samples, the background between 20 and 30º2θ increases due to formation of amorphous material. This effect is least pronounced in the Italian bentonite. Moreover, the intensity of the 060 reflection decreases after grinding, but the reflection does not migrate.

More detailed information about the changes in the smectite structure after grinding was obtained from Fourier transform infrared (FTIR) spectroscopy (Fig. 2). The assignment of bands follows that of Farmer (1974), Madejová *et al.* (1994) and Bishop *et al.* (2002). In all smectites, the complex

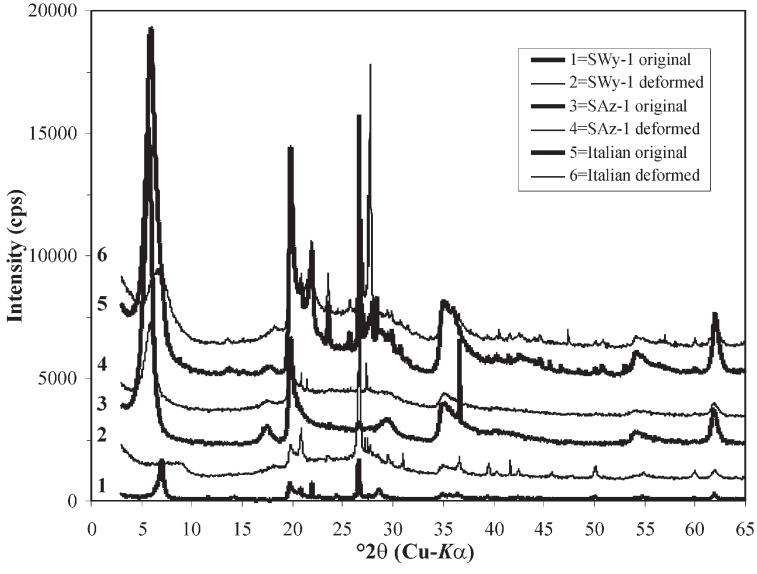

FIG. 1. XRD patterns of the original (bold) and the mechanically deformed smectites.

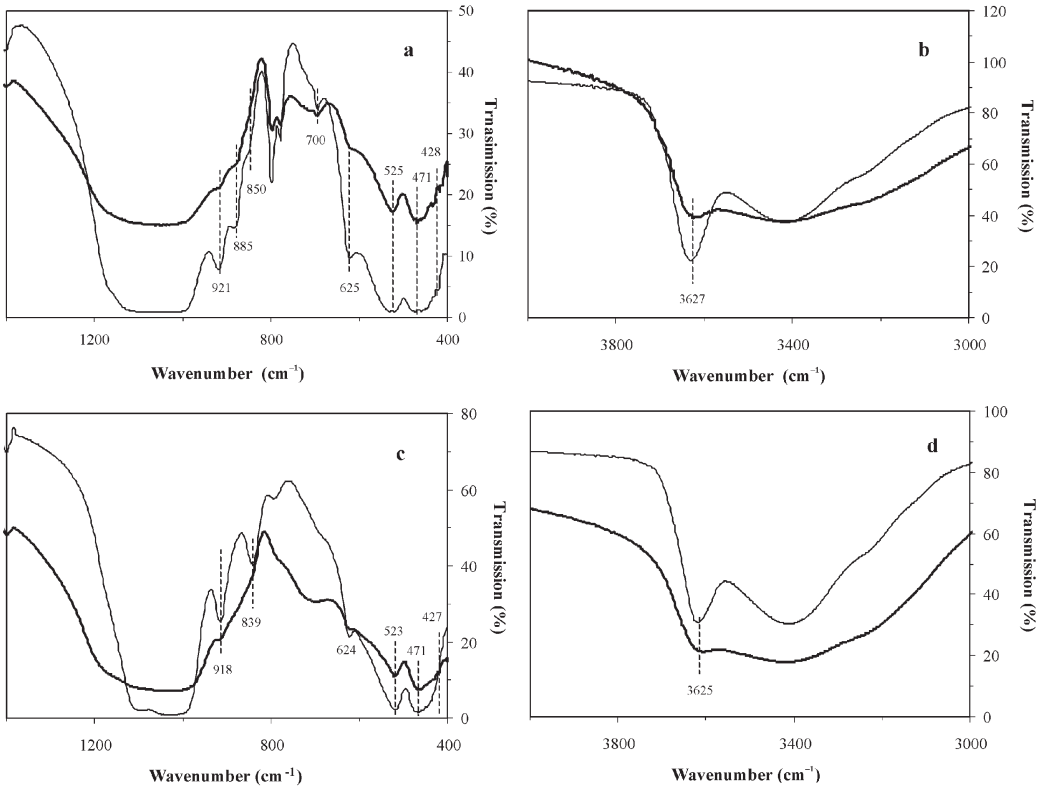

FIG. 2. FTIR spectra of the original and mechanically deformed (bold) smectites. (a,b) SWy-1; (c,d) SAz-1.

band centred at ~3625 cm^{-1}, with contributions from two AlAlOH stretching modes at 3618 and 3635 cm^{-1} and an AlMgOH stretching mode at 3602 cm^{-1} (Madejová *et al.*, 1994) decreases significantly with grinding. In the OH-bending region, the AlMgOH-bending vibration at ~845–850 cm^{-1} almost disappears. This is better observed in the case of the SAz-1 smectite. In contrast, the AlAlOH bending and especially the AlFeOH bending vibrations at 915–920 cm^{-1} and 880–885 cm^{-1}, respectively, are affected to a lesser degree by grinding. Lesser modifications are observed in the lattice-deformation bands. Thus, the bands at 524 cm^{-1}, 471 cm^{-1} and 428 cm^{-1} (Al-O-Si deformation, Si-O-Si deformation and Si-O bend, respectively) are slightly affected by grinding, in general becoming broader than their counterparts of the original bentonites. Similarly the Si-O stretching region (1000–1200 cm^{-1}) broadens.

The thermal analysis data (Fig. 3) show that the area of the dehydroxylation endotherm decreases significantly and migrates to slightly lower temperatures (Italian bentonite, SWy-1) or disappears (SAz-1). Only the TG-differential thermogravimetric (DTG) results are given, because the DTA curves are identical to the DTG curves. In the original samples, the weight loss is stepwise, whereas the ground samples display a gradual weight loss. In both the original and the ground samples the low-temperature endothermic peak, corresponding to the removal of water adsorbed mainly in the interlayer region, forms a doublet. Both components of this endothermic doublet shift to higher temperatures in the ground samples. Since the total weight loss remains essentially constant after grinding (Fig. 3) it follows that the relative importance of the adsorbed or bound, low-temperature water increases, while that of the crystalline water decreases with grinding.

The CEC of all bentonites decreases after grinding (Table 1). As expected, the decrease of the CEC follows the structural deformation of smectite and the degree of amorphization. The Italian bentonite, which is the least affected by

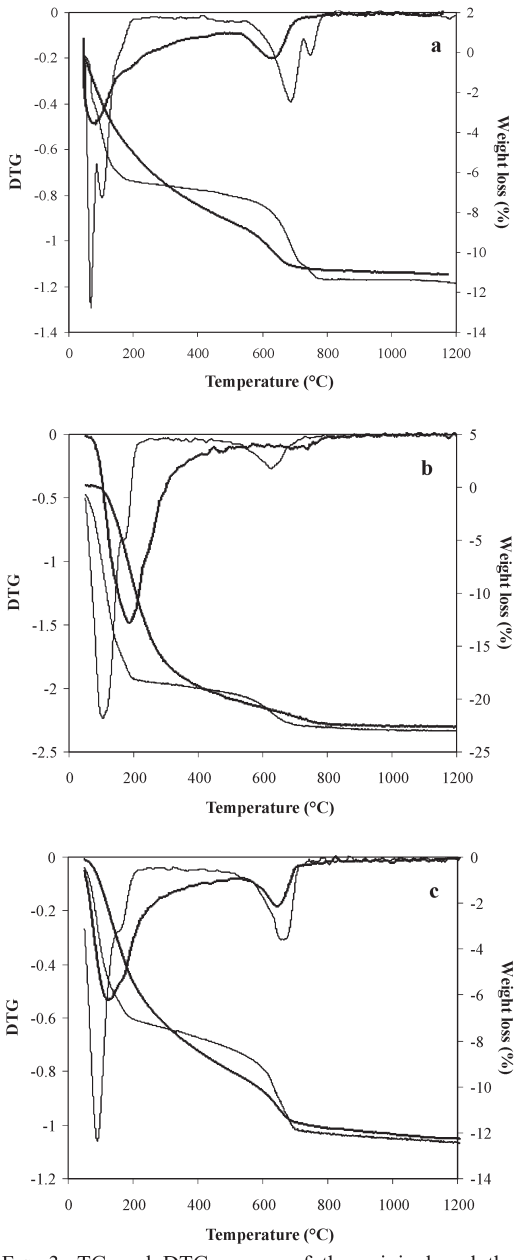

FIG. 3. TG and DTG curves of the original and the mechanically deformed (bold lines) smectites: (a) SWy-1; (b) SAz-1; and (c) Italian smectite.

grinding (Figs 1, 2), displays the smallest decrease in CEC. By contrast, SWy-1 and SAz-1, characterized by amorphization after grinding, display the maximum decrease in CEC. In the case of SWy-1, the CEC decreases by 50%. The destruction of the smectite structure involves a decrease of the smectite layer charge as well. In the Italian smectite the layer charge decreases from −0.450 to −0.429 moles of charge p.h.f.u., i.e. by 5% (Table 1). Therefore, the observed decrease in the CEC is attributed both to the amorphization and to the decrease in the layer charge. In SAz-1 it was not possible to determine the layer charge of the ground sample due to the lack of the 003 peak, but the migration of the 001 reflection to 16.5 Å (14 Å in the original sample) allowed an independent estimate of the proportion of the low-charge layers (c.f. Christidis & Eberl, 2003). This determination showed that the proportion of the low-charge layers increased from 10% in the original smectite to ~50% in the ground smectite, suggesting that the total layer charge of the ground SAz-1 smectite has decreased as well. If it is assumed that most of the high-charge layers (i.e. 75%) were preferentially destroyed as indicated by the almost total disappearance of the AlMgOH bending band (Fig. 2) then the layer charge of the ground SAz-1 sample is estimated to be −0.439 moles of charge p.h.f.u., suggesting a 20% decrease in the layer charge during grinding. Hence, in the Italian and the SAz-1 bentonite 50−60% of the observed decrease in the CEC is attributed to the decrease of the layer charge. In contrast, it was not possible to evaluate any possible decrease in the layer charge of SWy-1 because the layer charge of this sample is within the lower detection limit of the technique used.

Influence of grinding on SSA and porosity

The SSAs of the bentonites are listed in Table 2, and complete nitrogen gas adsorption-desorption isotherms are shown in Fig. 4. All original materials display type-II isotherms, which are typical of non-porous or macroporous adsorbents (Sing *et al.*, 1985). Mechanical deformation has caused significant decrease of the specific surface area and the volume of N_2 gas adsorbed. The adsorption isotherm of the deformed SAz-1 has been significantly affected by grinding and changed to a type-III isotherm. Such an isotherm indicates a weaker tendency for interaction with nitrogen gas molecules (Gregg & Sing, 1982). The adsorption-desorption isotherms of the Italian bentonite have been slightly affected by grinding, and the SWy-1 bentonite displays an intermediate behaviour. Both the SWy-1 and Italian bentonites display type-II

TABLE 1. CEC, layer charge and charge distribution of the original and the deformed bentonites.

Sample	CEC (mEq/100 g)	Layer charge (moles of charge p.h.f.u.)	Charge heterogeneity†
SWy-1 original	75.9	0.39	1/0/0
SWy-1 deformed	38.5	n.d.	n.d.
SAz-1 original	118.9	0.548	0.1/0.5/0.4
SAz-1 deformed	80.8	0.439*	0.5/0.4/0.1
Italian original	88.2	0.450	0.6/0/0.4
Italian deformed	77.1	0.429	0.75/0/0.25

n.d. – not determined
* estimated (see text for details)
† *x/y/z* = proportion of the low-charge (*x*), intermediate-charge (*y*) and high-charge (*z*) layers.

isotherms after grinding. Modifications in pore-size distribution of the three bentonites after mechanical deformation are shown in Fig. 5. Except for SAz-1 bentonite, the meso- and microporosity are not affected to a significant degree by mechanical deformation. In general, a slight decrease in both micro and mesoporosity is observed. In contrast, the SAz-1 bentonite displays a significant decrease in microporosity.

The significant decrease in microporosity of the mechanically deformed SAz-1 bentonite is clearly illustrated in the *t*-plots (Fig. 6, Table 2). A *t*-plot is a plot of the volume of gas adsorbed versus *t*, the statistical thickness of an adsorbed film, and is used for quantitative evaluation of microporosity (Sing *et al*., 1985). In this study *t* (Å) was determined by means of the de Boer equation:

$$t(\text{Å}) = \left[\frac{13.99}{0.034 + \log\left(\frac{P_0}{P}\right)} \right]^{1/2}$$

In general, only a fraction of the surface area of the bentonites accessible to N_2 gas is attributed to micropores (Table 2, Fig. 6). Nevertheless, in the original SAz-1, ~60% of the SSA is attributed to micropores, but this is destroyed during mechanical deformation.

Results from particle-size analysis using laser diffraction and particle-size distribution (PSD) curves are shown in Table 3 and Fig. 7, respectively. In all samples, particle size increases after mechanical deformation due to particle agglomeration; this can be attributed to cold welding (Gregg, 1968). The original samples are characterized by bimodal particle-size distributions, and the ground samples display multimodal size distribution, indicating the existence of several populations. The PSD of SWy-1 is dominated by a population centred at 7.5 μm, followed by a second coarser population centered at 45 μm. The PSD of the deformed SWy-1 is characterized by two additional coarse populations, one centred at 250 μm and a fine-grained population centred at 0.5 μm. Moreover, the relative abundance of the original

TABLE 2. Total SSA, external surface area, micropore surface area and micropore volume of the original and the mechanically deformed bentonites.

Sample	Specific surface area ($m^2\ g^{-1}$)	External surface area ($m^2\ g^{-1}$)	Micropore surface area ($m^2\ g^{-1}$)	Micropore volume ($cm^3\ g^{-1}$)
SWy-1 original	24.9	16.1	8.8	0.0045
SWy-1 deformed	16.4	12.1	4.3	0.0021
SAz-1 original	70.1	32.3	37.8	0.0192
SAz-1 deformed	24.8	19.9	4.9	0.0023
Italian original	36.8	33.3	3.5	0.0053
Italian deformed	31.9	25.7	6.2	0.0031

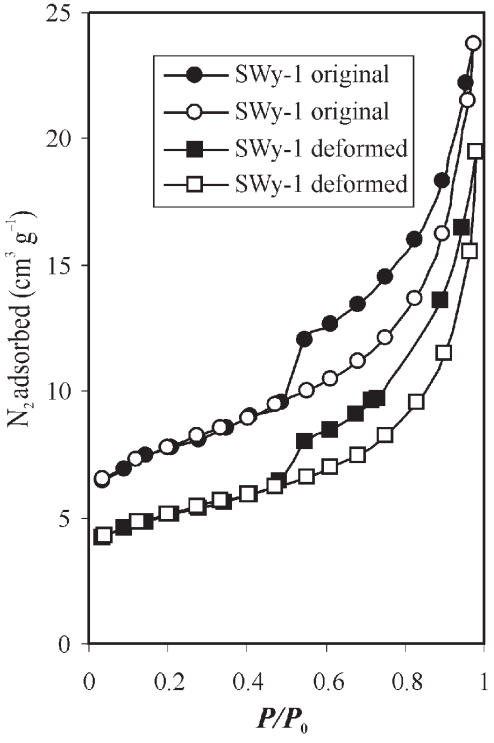

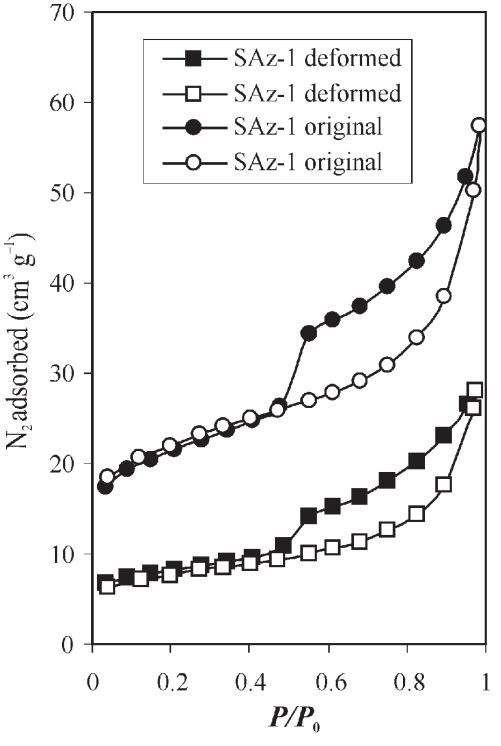

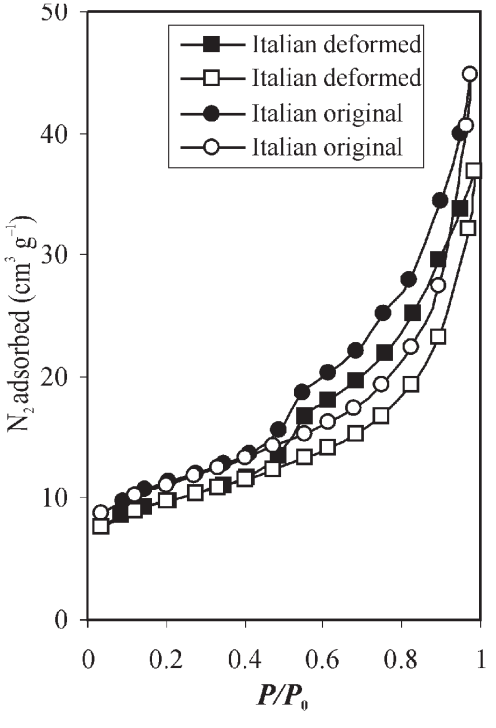

FIG. 4. Adsorption-desorption isotherms of the original and the mechanically deformed smectites.

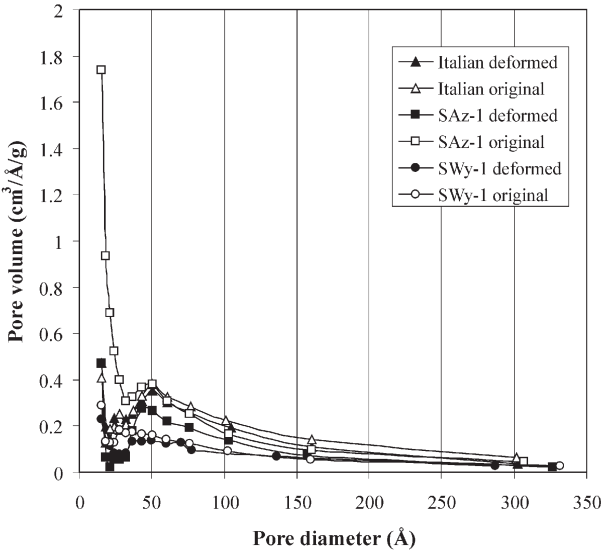

FIG. 5. Pore-size distribution of the original and the mechanically deformed smectites.

populations is reversed (Fig. 7a). The PSD of SAz-1 is also bimodal, dominated by a coarser population centred at 22.5 μm and a finer population centred at 5.5 μm. After grinding, the coarser population shifts to 30.5 μm but the fine-grained population remains unchanged, although its relative abundance decreases. Moreover, a finer population centred at 0.5 μm is also present. Finally, the Italian bentonite is characterized by a bimodal distribution with centres at 19 and 7.5 μm. After grinding, the coarse population shifts to 48 μm and the fine-grained population shifts to 2.5 μm. Similarly to the previous samples, a finer-grained population centred at 0.5 μm appears in the ground sample. A comparable PSD for a Sardinian bentonite was presented by Dellisanti & Valdre, (2005).

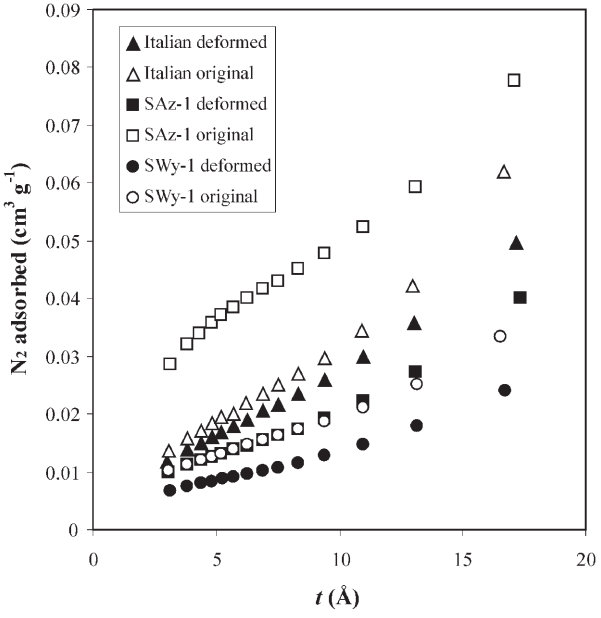

FIG. 6. *t*-plots of the original and the mechanically deformed smectites.

TABLE 3. Particle size (μm) distribution data (standard percentile readings, and mean equivalent spherical diameter (D[4,3])) of the original and the deformed bentonites.

Sample	D (v. 0.1)	D (v. 0.5)	D (v. 0.9)	D [4,3]
SWy-1 original	1.65	4.84	14.49	7.60
SWy-1 deformed	2.22	23.42	120.32	46.31
SAz-1 original	2.96	14.36	44.81	19.83
SAz-1 deformed	2.15	20.60	57.83	25.77
Italian original	2.35	10.75	34.98	15.25
Italian deformed	3.61	31.54	106.16	45.16

D (v. 0.1), D (v. 0.5), D (v. 0.9), are the mean particle sizes of 10%, 50% and 90% of the particles, respectively.

DISCUSSION

Mechanical deformation, after grinding under controlled conditions, of the three bentonites containing smectites with different layer charge, modified the structure of smectites: (1) by destruction of the smectite crystallites causing variable degrees of amorphization; (2) by decrease in the layer charge of the smectites; and (3) by agglomeration of the smectite grains. In all bentonites, size-distribution curves shifted to higher average grain size and additional particle populations formed after grinding. Although it is expected that grinding will produce a considerable amount of fines, the proportion of fine-grained material is not significant. Therefore, it is believed that particle agglomeration (cold welding) has also affected the fine-grained amorphous matter that probably formed during grinding. Moreover, it has decreased the SSA and the micro- and mesoporosity of the bentonites.

An interesting finding of this work is the decrease in the layer charge of smectites after mechanical deformation. The bentonites examined contain three different smectites with variable layer charge, and charge heterogeneity both in magnitude and localization. The FTIR results indicate that the decrease in layer charge is mostly related to the destruction of those octahedra filled by Mg. This is the reason for the considerable decrease in layer charge in the case of Mg-rich SAz-1. In contrast, those octahedra occupied by Fe have been least affected by grinding. Therefore, it seems that the Mg-bearing octahedra display minimum stability during mechanical deformation, probably due to the increasing strain imposed on the smectite lattice by the substitution of Mg for Al. Such a strain is expected if the difference in the ionic radii between Al and Mg is taken into account (cf. Radoslovich, 1962; Brownlow, 1996). Using the same reasoning, the resistance of Fe-bearing octahedra to structure collapse can be explained by the similarity of the ionic radii between Fe^{3+} (low spin state) and Al (Brownlow, 1996). If it is considered that deformation begins from the edges of the smectite crystallites, then it should involve the two tetrahedral sheets and those exposed octahedra occupied by Mg. Subsequent removal of Mg-bearing octahedra exposes new octahedra and Si-tetrahedra, which in turn are destroyed, thus forming excess amorphous matter (Fig. 8). The rate of octahedral sheet destruction is hindered when Fe-bearing octahedra are exposed to the mechanical activity of the ball mill.

The response of smectites to the mechanical deformation does not seem to be controlled by the magnitude of layer charge, because the Italian smectite, a typical smectite with an intermediate charge, is more stable than high- and low-charge smectites. The data obtained suggest that a significant proportion of tetrahedral charge seems to favour mechanical deformation and so does a large abundance of octahedral Mg. Hence it is expected that beidellite and nontronite will be more sensitive to grinding than Mg-rich montmorillonite. Additional work with different types of dioctahedral smectites, showing variable layer charge and charge distribution is required to verify this suggestion.

CONCLUSIONS

Extensive grinding of three bentonites (SWy-1, SAz-1 and an Italian bentonite) for 20 h under medium vacuum of 0.13 Pa and controlled temperature conditions (25ºC) caused mechanical deforma-

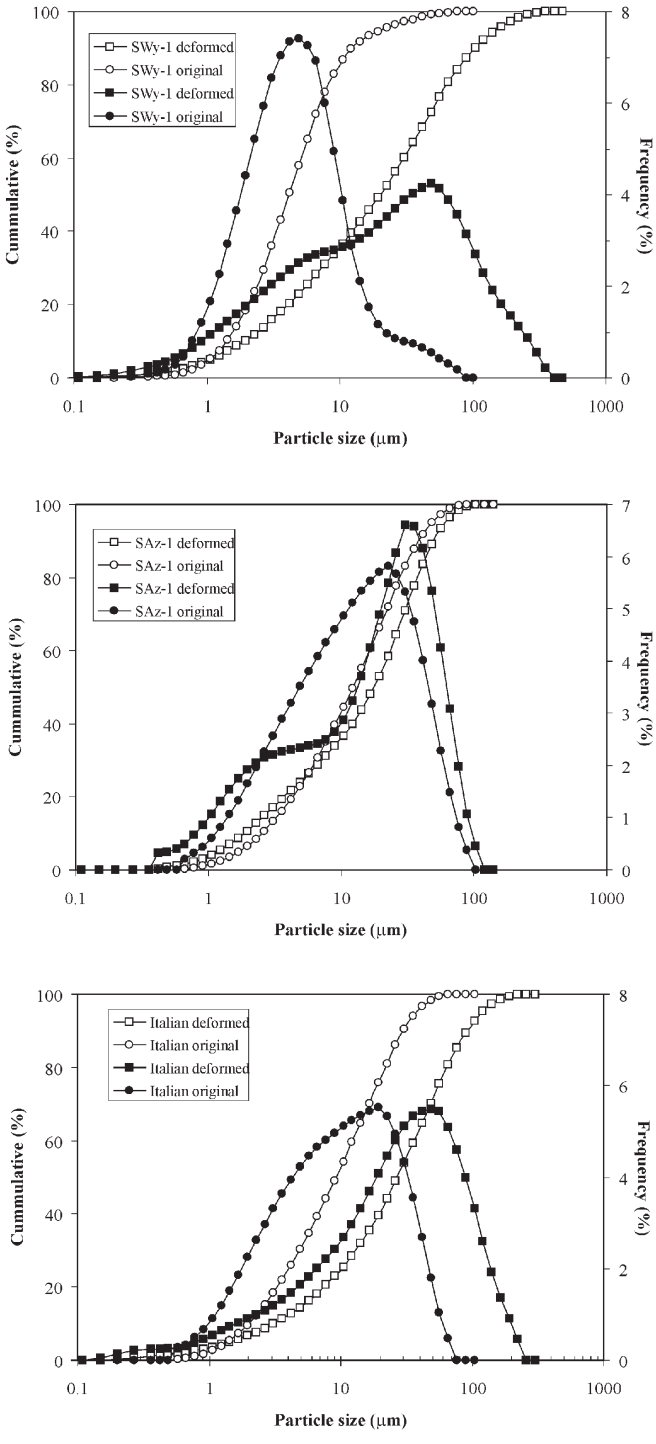

FIG. 7. Cumulative (empty symbols) and frequency (full symbols) particle-size distribution curves of the original and the mechanically deformed smectites.

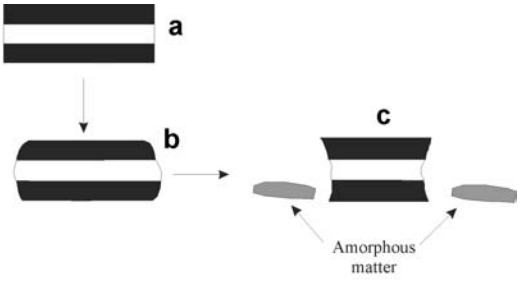

FIG. 8. Schematic representation of the mechanical deformation of the smectite crystallites and the formation of amorphous material during grinding: (a) original crystallite, (b) deformation begins in the tetrahedral sheet and to a lesser degree in the exposed surfaces of the octahedral sheet and exposes new surfaces from the octahedral sheet, (c) the exposed octahedral sheet is destroyed and new surfaces from the tetrahedral sheet are exposed. This process forms amorphous matter.

tion of the smectites. The modifications involve destruction of the smectite crystallites associated with variable degree of amorphization, decrease in the layer charge of smectites and agglomeration of the smectite grains (cold welding). The structural deformation is affected by the Mg-for-Al substitution in the octahedral sheet. In contrast, those octahedral sheets occupied by Fe are least affected by grinding. The structural modifications are associated with a decrease in the SSA, and the meso- and microporosity of the bentonites.

REFERENCES

Allen T. (1990) *Particle Size Measurement*. Vol. 1. Chapman & Hall, London, pp. 44–111.

Bishop J., Madejová J., Komadel P. & Fröschl H. (2002) The influence of structural Fe, Al and Mg on the infrared OH bands in spectra of dioctahedral smectites. *Clay Minerals*, **37**, 607–616.

Bonetti E., Campari E.G., Pasquini L., Sampaolesi E. & Valdrè G. (1998) Structural and elastic properties of nanocrystalline iron and nickel prepared by ball milling in a controlled thermodynamic environment. *Materials Science Forum*, **269–273**, 1005–1010.

Brandenburg U. & Lagaly G. (1988) Rheological properties of sodium montmorillonite dispersions. *Applied Clay Science*, **3**, 263–279.

Brownlow A.H. (1996) *Geochemistry*, 2nd edition. Prentice Hall International, London, pp. 239–295.

Brunauer S., Emmett P.H. & Teller E. (1938) Adsorption of gases in multimolecular layers. *Journal of the American Chemical Society*, **60**, 309–319.

Christidis G.E. & Eberl D.D. (2003) Determination of layer charge characteristics of smectites. *Clays and Clay Minerals*, **51**, 644–655.

Christidis G.E., Makri P. & Perdikatsis V. (2004) Influence of grinding on the structure and colour properties of talc, bentonite and calcite white fillers. *Clay Minerals*, **39**, 163–175.

Čičel V. & Kranz G. (1981) Mechanism of montmorillonite structure degradation by percussive grinding. *Clay Minerals*, **16**, 151–162.

Dellisanti F. & Valdre G. (2005) Study of structural properties of ion treated and mechanically deformed commercial bentonite. *Applied Clay Science*, **28**, 233–244.

Farmer V.C. (1974) The layer silicates. Pp. 331–363 in: *The Infrared Spectra of Minerals* (V.C. Farmer, editor). Monograph **4**, Mineralogical Society, London.

Gregg S.J. (1968) Surface chemical study of comminuted and compacted solids. *Chemistry and Industry*, **11**, 611–617.

Gregg S.J. & Sing K.S.W. (1982) *Adsorption, Surface Area and Porosity.* Academic Press, London, pp. 248–282.

Güven N. (1988) Smectite. Pp. 497–559 in: *Hydrous Phyllosilicates*. (S.W. Bailey, editor). Reviews in Mineralogy, **19**, Mineralogical Society of America, Washington D.C.

Kristoff E., Zoltan Juhasz A. & Vassanyi I. (1993) The effect of mechanical treatment on the crystal structure and thermal behavior of kaolinite. *Clays and Clay Minerals*, **41**, 608–612.

Liao J. & Senna M. (1992) Thermal behavior of mechanically amorphized talc. *Thermochimica Acta*, **197**, 295–306.

Madejová J., Komadel P. & Čičel B. (1994) Infrared study of octahedral site populations in smectites. *Clay Minerals*, **29**, 319–326.

Mingelgrin U., Kliger L., Gal M. & Saltzman S. (1978) The effect of grinding on the structure and behavior of bentonites. *Clays and Clay Minerals*, **26**, 299–307.

Mukherjee D.K. & Roy S. (1973) Effect of dry grinding on the CEC of some Indian Talcs. *Industrial Ceramics*, **10**, 215–219.

Newman A.C.D. & Brown G. (1987) The chemical constitution of clays. Pp 1–128 in: *Chemistry of Clays and Clay Minerals* (A.C.D Newman editor). Monograph **6**, Mineralogical Society, London.

Perez-Rodriguez J.L. & Sanchez-Soto P.J. (1991) The influence of the dry grinding on the thermal behavior of pyrophyllite. *Journal of Thermal Analysis*, **37**, 1401–1423.

Pietracaprina A., Novelli G. & Rinaldi A. (1971) Bentonite deposit at Uri, Sardinia, Italy. *Clay Minerals*, **9**, 351–355.

Radoslovich E.W. (1962) The cell dimensions and symmetry of layer-lattice silicates. II. Regression relations. *American Mineralogist*, **47**, 617–636.

Reynolds Jr. R.C. & Bish D.L. (2002) The effects of grinding on the structure of a low-defect kaolinite. *American Mineralogist*, **87**, 1626–1630.

Sanchez-Soto P.J., Wiewióra A., Aviles M.A, Justo A., Perez-Maqueda L.A., Perez-Rodriquez J.L. & Bylina P. (1997) Talc from Puebla de Lillo, Spain. II. Effect of dry grinding on particle size and shape. *Applied Clay Science*, **12**, 297–312.

Schultz L.G. (1969) Lithium and potassium adsorption, dehydroxylation temperature and structural water content of aluminous smectites. *Clays and Clay Minerals*, **17**, 115–149.

Scott P.W. (1990) *Brightness and Colour measurement*. CEC/ASEAN training course on assessment procedures for clays and ceramic raw materials. 11 pp.

Sing K.S.W., Everett D.H., Haul R.A.W., Moscou L., Pierotti R.A., Rouquerol J. & Siemieniewska T. (1985) Reporting physisorption data for gas/solid systems with special reference to the determination of surface area and porosity. *Pure and Applied Chemistry*, **57**, 603–619.

Stepkowska E.T., Perez-Rodriguez J.L., Himenez de Haro M.C., Sanchez-Soto P.J. & Maqueda L.A. (2001) Effect of grinding and water vapour on the particle size of kaolinite and pyrophyllite. *Clay Minerals*, **36**, 105–114.

Suraj G., Iyer C.S.P., Rugmini S. & Lalithambika M. (1997) The effect of micronization on kaolinites and their sorption behaviour. *Applied Clay Science*, **12**, 111–130.

Uhlik P., Šuchá V., Eberl D.D., Puškelová L'. & Čaplovičová M. (2000) Evolution of pyrophyllite particle sizes during dry grinding. *Clay Minerals*, **35**, 423–432.

Valdrè G., Zacchini D., Berti R., Costa A., Alessandrini A., Zucchetti P. & Valdrè U. (1999) Nitrogen sorption tests, SEM-Windowless EDS and XRD analysis of mechanically alloyed nanocrystalline getters materials. *Nanostructured Materials*, **11**, 821–829.

Volzone C., Aglietti E.F., Scian A.N. & Porto Lopez J.M. (1987) Effect of induced structural modifications on the physicochemical behavior of bentonite. *Applied Clay Science*, **2**, 97–104.

Wiewióra A., Sanchez-Soto P.J., Aviles M.A., Justo A. & Perez-Rodriguez J.L. (1993) Effect of dry grinding and leaching on polytypic structure of pyrophyllite. *Applied Clay Science*, **8**, 261–282.

Wills B.A. (1988) *Mineral Processing Technology*, 2nd edition. Pergamon Press, Oxford, UK, pp. 200–212.